IUCrJ
ISSN 2052-2525
MATERIALS | COMPUTATION

Spin-reorientation magnetic transitions in Mn-doped $SmFeO_3$

Jian Kang,[a] Yali Yang,[a] Xiaolong Qian,[a] Kai Xu,[a] Xiaopeng Cui,[a] Yifei Fang,[a] Venkatesh Chandragiri,[a] Baojuan Kang,[a] Bin Chen,[b] Alessandro Stroppa,[a,c] Shixun Cao,[a,d] Jincang Zhang[a,d] and Wei Ren[a,d]*

[a]Department of Physics, International Center of Quantum and Molecular Structures and Materials Genome Institute, Shanghai University, Shanghai 200444, People's Republic of China, [b]Hangzhou Key Laboratory of Quantum Matter, Department of Physics, Hangzhou Normal University, Hangzhou 310036, People's Republic of China, [c]CNR-SPIN, L'Aquila, Italy, and [d]Shanghai Key Laboratory of High-Temperature Superconductors, Shanghai University, Shanghai 200444, People's Republic of China. *Correspondence e-mail: renwei@shu.edu.cn

Received 4 April 2017
Accepted 29 May 2017

Edited by Y. Murakami, KEK, Japan

Keywords: spin reorientation transitions; rare earth perovskites; magnetic phase transitions; Mn doping.

Spin reorientation is a magnetic phase transition in which rotation of the magnetization vector with respect to the crystallographic axes occurs upon a change in the temperature or magnetic field. For example, $SmFeO_3$ shows a magnetization rotation from the *c* axis above 480 K to the *a* axis below 450 K, known as the $\Gamma_4 \rightarrow \Gamma_2$ transition. This work reports the successful synthesis of the new single-crystal perovskite $SmFe_{0.75}Mn_{0.25}O_3$ and finds interesting spin reorientations above and below room temperature. In addition to the spin reorientation of the $\Gamma_4 \rightarrow \Gamma_2$ magnetic phase transition observed at around T_{SR2} = 382 K, a new spin reorientation, $\Gamma_2 \rightarrow \Gamma_1$, was seen at around T_{SR1} = 212 K due to Mn doping, which could not be observed in the parent rare earth perovskite compound. This unexpected spin configuration has complete antiferromagnetic order without any canting-induced weak ferromagnetic moment, resulting in zero magnetization in the low-temperature regime. *M*–*T* and *M*–*H* measurements have been made to study the temperature and magnetic-field dependence of the observed spin reorientation transitions.

1. Introduction

The emerging demand for next-generation spintronic devices calls for more functional materials with outstanding properties. In this context, the $RFeO_3$ (*R* = rare earth ion) oxide family with the *Pbnm* structure are promising candidates, in which not only the magnetic interactions between the 3*d* spins of the transition metals (Fe–Fe) but also those with the 4*f* moments of the rare earth ions (*R*–Fe) have important roles in their magnetic behaviour and magnetoelectric coupling (Zvezdin & Mukhin, 2009). Up to now, $RFeO_3$ compounds have been investigated for future applications such as inertia-driven spin switching (Kimel *et al.*, 2009), laser-induced spin reorientation (SR) (de Jong *et al.*, 2011), ultrafast manipulation of spins through thermally induced SR transition (de Jong *et al.*, 2012), temperature and magnetic field control of SR (Cao *et al.*, 2014; Hong *et al.*, 2011; Cao *et al.*, 2016; Zhao *et al.*, 2015; Wu *et al.*, 2014; Wang *et al.*, 2016; Yuan *et al.*, 2013) and large rotating-field entropy change (Cao *et al.*, 2016; Huang *et al.*, 2013). The $RMnO_3$ family also draws a lot of attention due to spontaneous electric polarizations induced by noncollinear spiral magnetic order (Kenzelmann *et al.*, 2005), a collinear *E*-type antiferromagnetic structure (Okuyama *et al.*, 2011) and strong antiferromagnetic pinning effects (Jin *et al.*, 2015). In $RFeO_3$ and $RMnO_3$ compounds, below their Néel tempera-

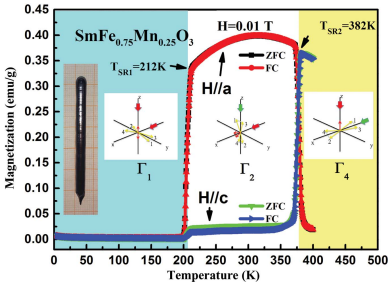

tures (T_N), the Fe^{3+} or Mn^{3+} sublattice will be ordered in a slightly canted antiferromagnetic configuration due to an antisymmetric exchange Dzyaloshinsky–Moriya interaction, while also showing weak ferromagnetism (Dzyaloshinsky, 1958; Moriya, 1960). Magnetoelectric (ME) coupling, which breaks spatial inversion and time-reversal symmetries (Mostovoy, 2006), has been the focus of extensive research to explore the mutual control of electric and magnetic degrees of freedom (Cao *et al.*, 2016; Fina *et al.*, 2010). Various magnetic phase transitions also occur in the presence of ME processes (Hemberger *et al.*, 2007; Kimura *et al.*, 2005) and dielectric properties may also change around the magnetic phase transition, thus providing an approach to trigger magnetodielectric coupling. It is worth noting that $DyFeO_3$ has been found experimentally to have a field-induced gigantic ME effect (Nakajima *et al.*, 2015). Consequently, the modification of magnetic and electric polarization by controlling the phase transition is the main theoretical and experimental objective to realise new multiferroic materials that have application at room temperature.

One of the special magnetic phase transitions in $RFeO_3$ which might be closely related to magnetically driven ferroelectricity is spin reorientation (SR). According to symmetry considerations and the antiferromagnetic nature of the coupling between the ions, there are three magnetic configurations allowed for the Fe^{3+} sublattice, namely Γ_1, Γ_2 and Γ_4, with different major antiferromagnetic directions (White, 1969). Complex R^{3+}–R^{3+}, R^{3+}–Fe^{3+} and Fe^{3+}–Fe^{3+} interactions can lead to competitive anisotropic magnetic features in $RFeO_3$, possessing slightly different free energies when the magnetic moments align along the three main axes over varying temperature ranges. For $RFeO_3$, the Γ_4 spin configuration appears in the higher temperature region, while the other two spin configurations can be found when the temperature is reduced (White, 1969). At extremely low temperatures a different spin configuration may appear, due to the more complicated ordering of sets of rare earth ions, such as observed in $TbFeO_3$ (Cao *et al.*, 2016) and $DyFeO_3$ (White, 1969).

$SmFeO_3$ has attracted much attention due to its intriguing behaviours, like fast magnetic switching (Jeong *et al.*, 2012), temperature-induced spin switching (Cao *et al.*, 2014), the highest SR temperature (T_{SR}) among the $RFeO_3$ system and its curious ferroelectric properties (Lee *et al.*, 2011; Kuo *et al.*, 2014). $SmMnO_3$ is one of the *A*-type antiferromagnetic (AFM) $RMnO_3$ compounds, showing negative magnetization (Cheng *et al.*, 2011) and magnetocapacitive effects (Jung *et al.*, 2010) as reported recently. In addition, the $RFe_xMn_{1-x}O_3$ (*R* = Dy, Tb and Y) family has been studied a lot due to their varying physical properties and interesting phase transitions (Nair *et al.*, 2016; Mandal *et al.*, 2013, 2011; Hong *et al.*, 2011). Typically, the usual way to control the temperature and configuration of the SR transition is to dope other lanthanides into $RFeO_3$, such as $Sm_{1-x}Dy_xFeO_3$ (Zhao *et al.*, 2015) and $Dy_{0.5}Pr_{0.5}FeO_3$ (Wu *et al.*, 2014). Here, we report a new way to change the SR transition by modifying the 3*d*–4*f* interaction between R^{3+}–Fe^{3+} with Mn^{3+} doping in single-crystal $SmFeO_3$. By doing so, we found that the $SmFe_xMn_{1-x}O_3$ family can possess novel properties that are absent from the parent $SmFeO_3$ and $SmMnO_3$ rare earth perovskites. Here, we focus our investigation on the twofold SR magnetic transitions of $SmFe_{0.75}Mn_{0.25}O_3$ and the continuously tunable phase transition as observed from the temperature dependence of the magnetization (*M*–*T*) under external applied fields and hysteresis loops (*M*–*H*).

2. Experimental

The $SmFe_{0.75}Mn_{0.25}O_3$ (SFMO) single crystal was grown by the optical floating-zone method (Crystal System Inc., model FZ-T-10000H-VI-P-SH). The compounds of the feed and seed rods were prepared by a solid-state reaction in which the stoichiometric starting materials were Sm_2O_3 (99.99%), Fe_2O_3 (99.9%) and MnO_2 (99.9%) in a properly mixed proportion of 4:3:2. The temperature of the molten zone was controlled by adjusting the power of four lamps. The molten zone moved upwards at a rate of 3 mm h^{-1}.

The crystallinity and crystallographic orientations were determined by X-ray Laue photography. The microstructure of the crystal was checked by X-ray diffraction using a Rigaku 18 kW D/MAX-2550 diffractometer (Cu $K\alpha$ radiation) with a scanning step of 0.02° and 2θ from 10° to 120°. The dc magnetization measurements were performed using a Physics Property Measurement System (Quantum Design, PPMS-9). Zero-field-cooling (ZFC) and field-cooling (FC) processes were used to acquire the temperature dependence of the magnetization.

3. Results

Fig. 1(*a*) shows the Rietveld refinement of powder X-ray diffraction (XRD) data from the single crystal of $SmFe_{0.75}Mn_{0.25}O_3$ performed using the *AutoFP* (Cui *et al.*, 2015) and *FULLPROF* (Rodríguez-Carvajal, 2001) programs. The diffraction patterns can be assigned to the single-phase orthorhombic perovskite structure with space group *Pbnm* and no impurity phases were detected. The lattice parameters thus obtained are a = 5.39392 Å, b = 5.63707 Å and c = 7.67156 Å (R_{wp} = 0.133). Fig. 1(*b*) shows the clear Laue diffraction spots, indicating the high quality of our

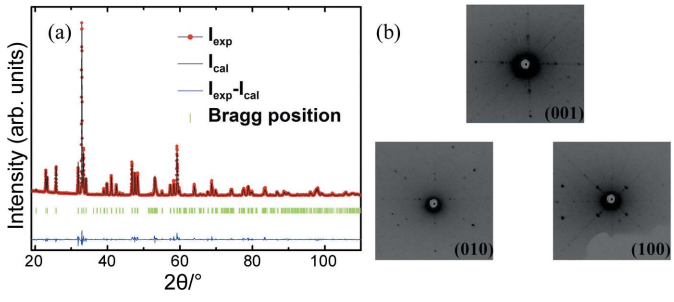

Figure 1
(*a*) X-ray diffraction pattern and (*b*) Laue back-scattering photography of $SmFe_{0.75}Mn_{0.25}O_3$ single crystal along the (001), (010) and (100) crystallographic axes.

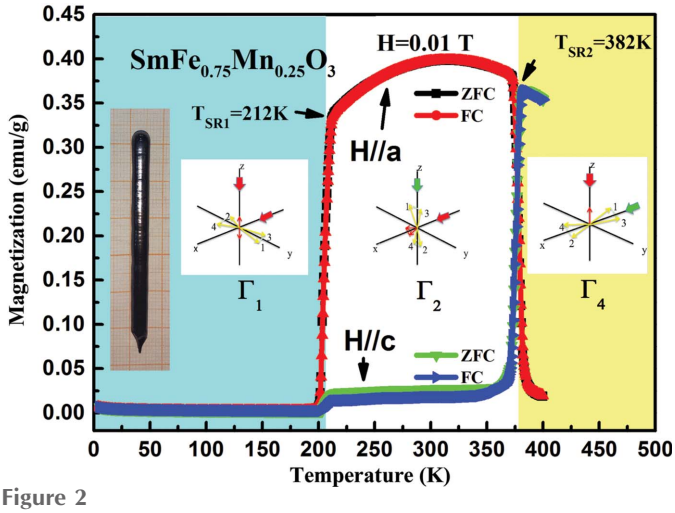

Figure 2
Temperature-dependent magnetizations of $SmFe_{0.75}Mn_{0.25}O_3$ along the *a* and *c* axes under magnetic field H = 0.01 T. Three slightly canted antiferromagnetic phases Γ_1, Γ_2 and Γ_4 can be distinguished by the shaded areas. The inset shows the $SmFe_{0.75}Mn_{0.25}O_3$ single-crystal sample.

$SmFe_{0.75}Mn_{0.25}O_3$ single crystal. Both XRD and Laue photography confirmed the excellent quality of the sample, and the cutting planes are precisely perpendicular to the *a*, *b* and *c* axes, respectively.

Fig. 2 shows the temperature dependence of the ZFC and FC magnetizations measured under a field of H = 0.01 T for the $SmFe_{0.75}Mn_{0.25}O_3$ single crystal (sample shown in the inset) along the the *a* and *c* axes, respectively. The second-order transition starting from T_{SR2} = 382 K is the first spin reorientation, where the Fe^{3+} spins reorient from a configuration of canting antiferromagnetism along the *a* axis with weak ferromagnetism along the *c* axis, $\Gamma_4(G_x, A_y, F_z)$, to canting antiferromagnetism along the *c* axis with weak ferromagnetism along the *a* axis, $\Gamma_2(F_x, C_y, G_z)$. Another unique and new feature of the *M*–*T* curve is that at T_{SR1} = 212 K, the $SmFe_{0.75}Mn_{0.25}O_3$ single crystal undergoes a second SR transition at a lower temperature with weak ferromagnetism along the *a* axis $\Gamma_2(F_x, C_y, G_z)$, changing to complete antiferromagnetism with no net magnetization, $\Gamma_1(A_x, G_y, C_z)$. This kind of SR behaviour has never been reported in the literature to the best of our knowledge.

The transition over the whole temperature range might be called a $\Gamma_4 \rightarrow \Gamma_2 \rightarrow \Gamma_1$ double SR transition. Since pure $SmFeO_3$ possesses a spin configuration from Γ_4 to Γ_2 due to the Sm^{3+}–Fe^{3+} interaction at rather high temperatures (450–480 K), it is reasonable to have such a spin configuration transition in $SmFe_{0.75}Mn_{0.25}O_3$ at a lower temperature of 361–382 K. The most interesting finding here is the spin configuration from Γ_2 to Γ_1 due to Mn^{3+} doping in $SmFeO_3$ that gives a vanishing effective moment vector below T_{SR1} = 212 K. It is known that there is no SR in the whole family of the $RMnO_3$ system. In addition, it is very rare for a rare earth orthoferrite to possess a Γ_1 spin configuration, with the exception of $DyFeO_3$ (Fu *et al.*, 2014), for which the SR transition temperature (T_{SR} = 37 K) is much lower than that of our single crystal here.

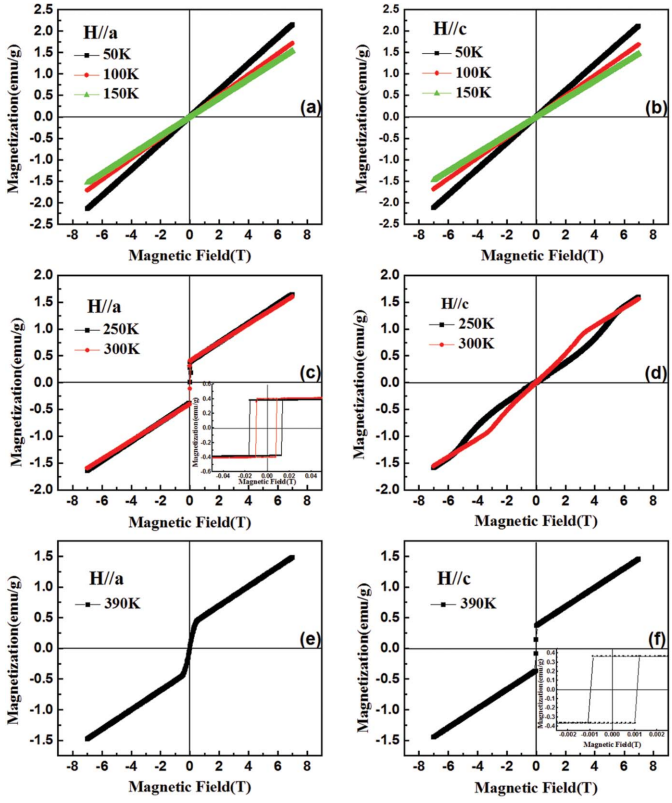

Figure 3
M–*H* curves for the $SmFe_{0.75}Mn_{0.25}O_3$ single crystal along the *a* and *c* axes at temperatures of (*a*), (*b*) 50 K, 100 K and 150 K, (*c*), (*d*) 250 K and 300 K, and (*e*), (*f*) 390 K. The insets of (*c*) and (*f*) show enlargements of the plots at small magnetic field.

To investigate the SR transition further, the *M*–*H* curves were measured at different temperatures along the *a* and *c* axes, repectively. Figs. 3(*a*) and 3(*b*) show the standard linear AFM behaviour at 50, 100 and 150 K with a change of slope, which corresponds to the feature of Γ_1 spin configuration below T_{SR1} = 212 K. Fig. 3(*c*) and inset show the uncompensated ferromagnetism component along the *a* axis, while Fig. 3(*d*) shows AFM-like behaviour but with noticeable kinks along the *c* axis. Above 382 K, the AFM-like and kink behaviour is more obviously seen in the *a* axis *M*–*H*, as shown in Fig. 3(*e*), while the *c* axis shows a ferromagnetism component in Fig. 3(*f*) and its inset. Inflexion behaviours are observed in Figs. 3(*d*) and 3(*e*) when the magnetic fields reach certain critical values, which suggests a field-induced SR. Therefore, according to Fig. 3, we can confirm that the weak ferromagnetism aligns along the *c* axis when the temperature is below T_N (around 600 K), and changes its direction to the *a* axis when the temperature drops below T_{SR2} = 382 K, before disappearing in any direction below T_{SR1} = 212 K, as shown in Fig. 2. Therefore, such a double SR transition induced by temperature is extraordinary for a single-phase rare earth perovskite.

Fig. 4(*a*) shows the *M*–*T* curves along the *c* axis when we change the magnitude of the external magnetic field. Upon increasing the magnetic field, T_{SR2} moves to a lower temperature in a linear-like fashion. For example, we can see

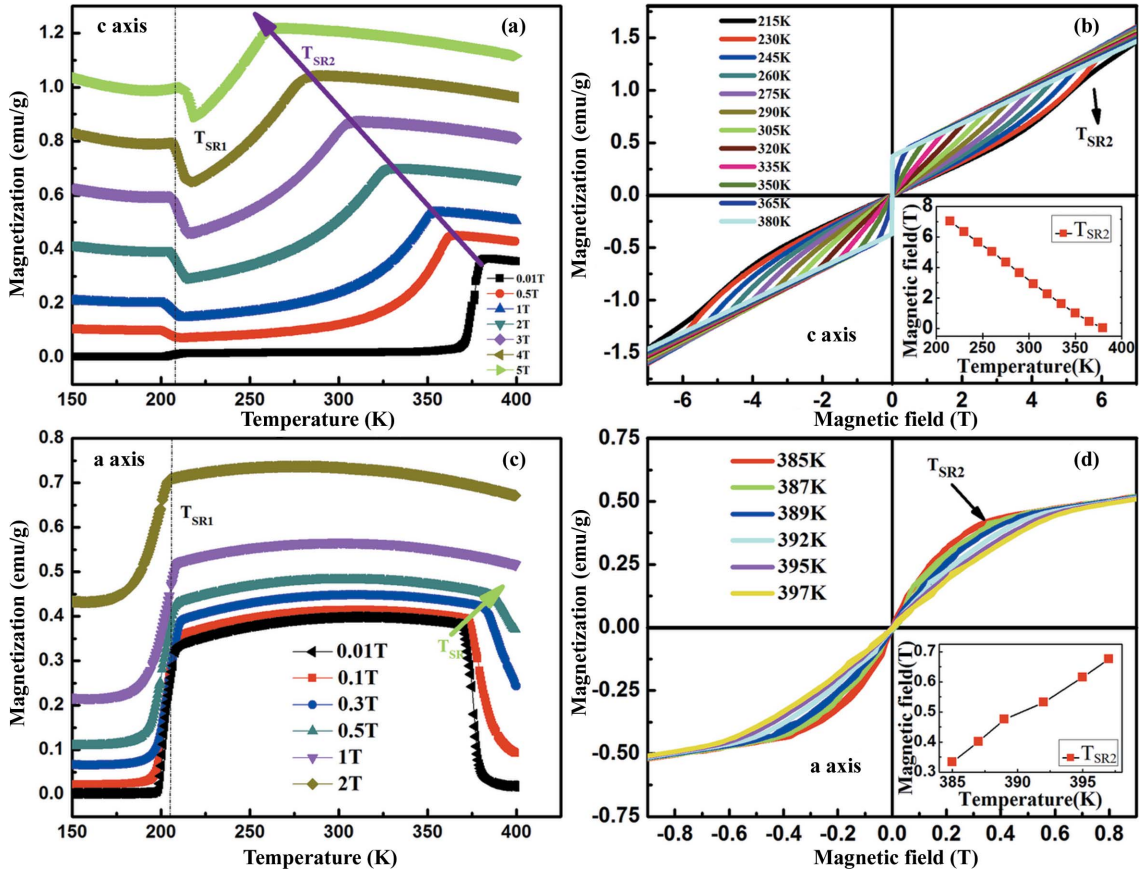

Figure 4
(*a*) *M*–*T* curves along the *c* axis at different magnetic fields from 0.01 to 5 T. (*b*) *M*–*H* curves along the *c* axis at different temperatures from 215 to 380 K. (*c*) *M*–*T* curves along the *a* axis at different magnetic fields from 0.01 to 2 T. (*d*) *M*–*H* curves along the *a* axis at different temperatures from 385 to 397 K. The insets in (*b*) and (*d*) show the linear temperature dependence of T_{SR2} along the *c* and *a* axes, respectively.

that the value of T_{SR2} decreases to 263 K under H = 5 T. Thus, we believe that when the magnetic field is high enough, the Γ_2 spin configuration will be totally suppressed. On the other hand, T_{SR1} is found to be almost constant regardless of the magnitude of the external field. Fig. 4(*b*) shows the measured *M*–*H* curves at different temperatures ranging from 215 to 380 K. This diagram shows the evolution of the *M*–*H* curves with a change of slope around T_{SR2} at different temperatures, illustrating an intermediate state between two different magnetic configurations, corroborating the details of Fig. 4(*a*). Here, the magnetic order would be stabilized in a Γ_4 spin configuration with a moment along the *c* axis after the intermediate state. Furthermore, we also observe from both Figs. 4(*a*) and 4(*b*) that, with increasing magnetic field, the inflection points move to low temperature. On the other hand, when we apply the external magnetic field along the *a* axis, Fig. 4(*c*) shows that the spin reorientation temperature T_{SR2} will move to the high-temperature region, as indicated by the green arrow. When the magnetic field exceeds 0.5 T, T_{SR2} moves above 400 K, which is beyond our temperature detection limit. Fig. 4(*d*) shows the *M*–*H* curves along the *a* axis at temperatures ranging from 385 to 397 K. The collected data show another linearly increasing behaviour for T_{SR2} *versus* magnetic field, consistent with that of the *M*–*T* curve in Fig. 4(*c*). In addition, T_{SR1} remains constant with varying magnetic field, as indicated by the vertical dashed line. To sum up, the Γ_4 to Γ_2 SR transition temperature can be easily controlled by magnetic field, whereas the Γ_2 to Γ_1 transition temperature is insensitive to the magnetic field.

4. Discussion

As mentioned, the rare earth orthoferrites have two kinds of magnetic ion, M^{3+} and R^{3+}. So there are three kinds of magnetic interaction, M^{3+}–M^{3+}, M^{3+}–R^{3+} and R^{3+}–R^{3+}. These three interactions all consist of isotropic, antisymmetric and anisotropic-symmetric super-exchange interactions, which inevitably makes the magnetic properties of RFeO$_3$ complex. Further, the antisymmetric and anisotropic-symmetric super-exchange interactions of M^{3+}–R^{3+} are responsible for the temperature-induced SR (Yamaguchi, 1974). In our case, the interaction becomes even more complicated due to the doping Mn^{3+} ions and intriguingly introduces all three spin configurations allowed in RFeO$_3$. By minimizing the free energy in the Γ_4 to Γ_2 SR transition with respect to θ and Φ (θ is the rotation angle of the easy axis in the *ac* plane and 2Φ represents the angle between two sublattices of the R^{3+} spins), one can obtain the following equation (Yamaguchi, 1974):

$$\left(J_B - J_C\right)\left(\hat{J} + \hat{J}'\right)^2 (s_0 + s\cos\Phi)\, s\sin\Phi + \left(J_D + J_B\right)\left(\hat{J} - \hat{J}'\right)^2 \times (s_0'\sin\theta - s\sin\Phi)\, s\cos\Phi = 0, \quad (1)$$

$$\cos\theta\left\{\left[2(D-E) + \frac{\left(D_z - C_z\right)^2}{2\left(J_D - J_C\right)} - \frac{\left(B_x - C_x\right)^2}{2\left(J_B - J_C\right)^2}\right]\sin\theta + 2s_0'\left[\frac{(\hat{J} - \hat{J}')^2}{\left(J_B - J_C\right)}\right] s\sin\Phi\right\} = 0 \quad (2)$$

where s is the ratio of the mean values of the R^{3+} and M^{3+} spins, $\langle S_R\rangle/\langle S_M\rangle$, which is the only parameter depending directly on temperature. The other parameters in equations (1) and (2) are different exchange constants. These two equations give the following three sets of solutions, (I), (II) and (III).

$$\text{(I)} \quad \sin\Phi = 0. \quad (3)$$

In this case, the stable angle of θ is 0 and this gives the Γ_4 configuration in the high-temperature phase (382 K < T < T_N).

$$\text{(II)} \quad s\cos\Phi = s_{c1}. \quad (4)$$

where

$$s_{c1} = \frac{-s_0[(\hat{J} + \hat{J}')^2/(J_D + J_B)]}{[(\hat{J} + \hat{J}')^2/(J_D + J_B)] + [(As_0' - 1)(\hat{J} - \hat{J}')^2/(J_B - J_C)]}, \quad (5)$$

and

$$A = \frac{-2s_0'[(\hat{J} - \hat{J}')^2/(J_B - J_C)]}{2(D-E) + [(D_z - C_z)^2/2(J_D - J_C)] - [(B_x - C_x)^2/2(J_B - J_C)^2]}. \quad (6)$$

The equilibrium values of θ can be acquired as

$$\theta = \sin^{-1}\{[A(s^2 - s_{c1}^2)^{1/2}]\}. \quad (7)$$

From equation (7), we can see that θ is zero when $s = s_{c1}$ and will increase with increasing s. This implies rotation of the spin system. When s reaches another critical value of $s = [s_{c1}^2 + (1/A^2)]^{1/2}$, θ will take a value of $\pi/2$. This process corresponds to the continuous SR intermediate range (361 K $\leq T \leq$ 382 K).

$$\text{(III)} \quad \cos\theta = 0. \quad (8)$$

This indicates that the easy axis has rotated to the c axis and the system is in the Γ_2 phase. Briefly, the case when $s = 0$ corresponds to the state at the Néel temperature. At high temperature s is small, and when $s \leq s_{c1}$ the free energy $F(\Gamma_4)$ is lower and the spin system will be stabilized in the Γ_4 configuration due to the anisotropic energy of the Fe^{3+} single ions. As the temperature decreases, the sublattice moments of Sm^{3+} and Fe^{3+} will increase and s gradually approaches s_{c1} where the free energy $F(\Gamma_{24})$ crosses $F(\Gamma_4)$. When s finally surpasses $[s_{c1}^2 + (1/A^2)]^{1/2}$, the free energy $F(\Gamma_2)$ becomes lowest, thus favouring the Γ_2 configuration. This is the typical continous SR transition in most RFeO$_3$ systems, but in the Mn^{3+}-doped SmFeO$_3$ single crystal the situation will become more complicated. Once the first SR transition is complete, the Mn^{3+} ions will be ordered with decreasing temperature and this will consequently influence the distribution of the free energy along the three main axes and s as well. When s reaches another critical value s_{c2}, the free energy of the Γ_1 configuration is smaller than that of Γ_2 and Γ_4, and the corresponding temperature is 212 K for our case.

So far, we have discussed two criticial values of s, namely s_{c1} and s_{c2}. For an un-doped RFeO$_3$ system, if $s_{c1} \leq s_{c2}$, a Γ_4 to Γ_2 SR transition will be seen, and if $s_{c1} \geq s_{c2}$, a Γ_4 to Γ_1 SR transition will occur (Yamaguchi, 1974). Indeed, if s never reaches s_{c1} or s_{c2} in the whole temperature range, no SR takes place, and this is the case for LaFeO$_3$ and YFeO$_3$. With the appropriate concentration of Mn^{3+}, the influence of the Mn^{3+} sublattice will make s grow more rapidly as the temperature decreases and s will reach s_{c2} at high temperature where the spin structure transforms to the Γ_1 configuration (Hornreich *et al.*, 1975).

The energy of an antiferromagnetic system in a magnetic field is lower when the antiferromagnetic vector is perpendicular to the direction of the field than when the two are parallel (Johnson *et al.*, 1980). A magnetic field applied along the antiferromagnetic axis of the Fe^{3+} system in the rare earth orthoferrites acts to cause reorientation of the Fe^{3+} antiferromagnetic vector to a perpendicular alignment. It is the competition between this Zeeman energy and the magnetic anisotropy energy of the Fe^{3+} system that determines the spin reorientation. In our case, since the antiferromagnetic vector of the Γ_1 configuration is along the b axis, one would not expect a field-induced change in the SR temperature T_{SR1} when the external field is along the c or a axis. Accordingly, a field-modified spin reorientation is seen when the external field is along the c axis rather than the a axis, as the antiferromagnetic vector of the Γ_2 configuration is along the c axis when the temperature is between T_{SR1} and T_{SR2}. Weak magnetism along the c-axis direction can be induced by applying an external field along the c axis. The Γ_4 configuration has its antiferromagnetic vector along the a axis, and an external field along the a axis can induce another Γ_2 spin configuration when the temperature is between T_{SR2} and T_N.

5. Conclusions

In summary, we have successfully synthesized a single crystal of $SmFe_{0.75}Mn_{0.25}O_3$, which has a single-phase perovskite structure, by the optical floating-zone method. The magnetic properties along different crystallographic axes have been studied in detail. Interesting double spin reorientation transitions $\Gamma_4 \rightarrow \Gamma_2 \rightarrow \Gamma_1$ were observed above and below room temperature. Field-induced spin reorientation has been investigated along the c and a axes in detail, showing the linear dependence and independence of SR temperatures *versus* magnetic field. Delicate interactions between the magnetic sublattices of Sm^{3+}, Fe^{3+} and Mn^{3+} make this unique compound highly sensitive to magnetic field and to temperature. Due to its intriguing magnetic characteristics, novel

magnetic switching devices could be designed based on this finding.

Funding information

Funding for this research was provided by: National Key Basic Research Program of China (award Nos. 2015CB921600, 2016YFB0700201); National Natural Science Foundation of China (award Nos. 51672171, 11574194, 51372149, 11274222); Eastern Scholar Program from Shanghai Municipal Education Commission; Shanghai Materials Genome Institute from the Shanghai Municipal Science and Technology Commission (award No. 14DZ2261200).

References

Cao, Y., Xiang, M., Zhao, W., Wang, G., Feng, Z., Kang, B., Stroppa, A., Zhang, J., Ren, W. & Cao, S. (2016). *J. Appl. Phys.* **119**, 063904.

Cao, S., Zhao, H., Kang, B., Zhang, J. & Ren, W. (2014). *Sci. Rep.* **4**, 5960.

Cheng, J. G., Zhou, J. S., Goodenough, J. B., Su, Y. T., Sui, Y. & Ren, Y. (2011). *Phys. Rev. B*, **84**, 104431.

Cui, X., Feng, Z., Jin, Y., Cao, Y., Deng, D., Chu, H., Cao, S., Dong, C. & Zhang, J. (2015). *J. Appl. Cryst.* **48**, 1581–1586.

Dzyaloshinsky, I. (1958). *J. Phys. Chem. Solids*, **4**, 241–255.

Fina, I., Fàbrega, L., Martí, X., Sánchez, F. & Fontcuberta, J. (2010). *Appl. Phys. Lett.* **97**, 232905.

Fu, X., Liu, X. & Zhou, J. (2014). *Mater. Lett.* **132**, 190–192.

Hemberger, J., Schrettle, F., Pimenov, A., Lunkenheimer, P., Ivanov, V. Y., Mukhin, A. A., Balbashov, A. M. & Loidl, A. (2007). *Phys. Rev. B*, **75**, 035118.

Hong, F., Cheng, Z., Zhao, H., Kimura, H. & Wang, X. (2011). *Appl. Phys. Lett.* **99**, 092502.

Hornreich, R. M., Komet, Y., Nolan, R., Wanklyn, B. M. & Yaeger, I. (1975). *Phys. Rev. B*, **12**, 5094–5104.

Huang, R., Cao, S., Ren, W., Zhan, S., Kang, B. & Zhang, J. (2013). *Appl. Phys. Lett.* **103**, 162412.

Jeong, Y. K., Lee, J.-H., Ahn, S.-J. & Jang, H. M. (2012). *Solid State Commun.* **152**, 1112–1115.

Jin, Y., Cui, X. P., Cheng, J. A., Cao, S. X., Ren, W. & Zhang, J. C. (2015). *Appl. Phys. Lett.* **107**, 072907.

Johnson, C. E., Prelorendjo, L. A. & Thomas, M. F. (1980). *J. Magn. Magn. Mater.* **15–18**, 557–558.

Jong, J. A. de, Kimel, A. V., Pisarev, R. V., Kirilyuk, A. & Rasing, T. (2011). *Phys. Rev. B*, **84**, 104421.

Jong, J. A. de, Razdolski, I., Kalashnikova, A. M., Pisarev, R. V., Balbashov, A. M., Kirilyuk, A., Rasing, T. & Kimel, A. V. (2012). *Phys. Rev. Lett.* **108**, 157601.

Jung, J.-S., Iyama, A., Nakamura, H., Mizumaki, M., Kawamura, N., Wakabayashi, Y. & Kimura, T. (2010). *Phys. Rev. B*, **82**, 212403.

Kenzelmann, M., Harris, A. B., Jonas, S., Broholm, C., Schefer, J., Kim, S. B., Zhang, C. L., Cheong, S. W., Vajk, O. P. & Lynn, J. W. (2005). *Phys. Rev. Lett.* **95**, 087206.

Kimel, A. V., Ivanov, B. A., Pisarev, R. V., Usachev, P. A., Kirilyuk, A. & Rasing, T. (2009). *Nat. Phys.* **5**, 727–731.

Kimura, T., Lawes, G., Goto, T., Tokura, Y. & Ramirez, A. P. (2005). *Phys. Rev. B*, **71**, 224425.

Kuo, C. Y. *et al.* (2014). *Phys. Rev. Lett.* **113**, 217203.

Lee, J. H., Jeong, Y. K., Park, J. H., Oak, M. A., Jang, H. M., Son, J. Y. & Scott, J. F. (2011). *Phys. Rev. Lett.* **107**, 117201.

Mandal, P., Bhadram, V. S., Sundarayya, Y., Narayana, C., Sundaresan, A. & Rao, C. N. R. (2011). *Phys. Rev. Lett.* **107**, 137202.

Mandal, P., Serrao, C. R., Suard, E., Caignaert, V., Raveau, B., Sundaresan, A. & Rao, C. N. R. (2013). *J. Solid State Chem.* **197**, 408–413.

Moriya, T. (1960). *Phys. Rev.* **120**, 91–98.

Mostovoy, M. (2006). *Phys. Rev. Lett.* **96**, 067601.

Nair, H. S., Chatterji, T., Kumar, C. M. N., Hansen, T., Nhalil, H., Elizabeth, S. & Strydom, A. M. (2016). *J. Appl. Phys.* **119**, 053901.

Nakajima, T., Tokunaga, Y., Taguchi, Y., Tokura, Y. & Arima, T. H. (2015). *Phys. Rev. Lett.* **115**, 197205.

Okuyama, D., Ishiwata, S., Takahashi, Y., Yamauchi, K., Picozzi, S., Sugimoto, K., Sakai, H., Takata, M., Shimano, R., Taguchi, Y., Arima, T. & Tokura, Y. (2011). *Phys. Rev. B*, **84**, 054440.

Rodríguez-Carvajal, J. (2001). *IUCr Commission Powder Diffr. Newsl.* **26**, 12–19.

Wang, G., Zhao, W., Cao, Y., Kang, B., Zhang, J., Ren, W. & Cao, S. (2016). *J. Alloys Compd.* **674**, 300–304.

White, R. L. (1969). *J. Appl. Phys.* **40**, 1061–1069.

Wu, H., Cao, S., Liu, M., Cao, Y., Kang, B., Zhang, J. & Ren, W. (2014). *Phys. Rev. B*, **90**, 144415.

Yamaguchi, T. (1974). *J. Phys. Chem. Solids*, **35**, 479–500.

Yuan, S. J., Ren, W., Hong, F., Wang, Y. B., Zhang, J. C., Bellaiche, L., Cao, S. X. & Cao, G. (2013). *Phys. Rev. B*, **87**, 180405.

Zhao, W., Cao, S., Huang, R., Cao, Y., Xu, K., Kang, B., Zhang, J. & Ren, W. (2015). *Phys. Rev. B*, **91**, 104425.

Zvezdin, A. K. & Mukhin, A. A. (2009). *JETP Lett.* **88**, 505–510.